




# Multi-omics Analysis Revealed Coordinated Responses of Rumen Microbiome and Epithelium to High-Grain-Induced Subacute Rumen Acidosis in Lactating Dairy Cows

Yingyu Mu,<sup>a,b</sup> Wangpan Qi,<sup>a,b</sup> Tao Zhang,<sup>a,b</sup> Jiyou Zhang,<sup>a,b</sup>  Shengyong Mao<sup>a,b</sup>

<sup>a</sup>Ruminant Nutrition and Feed Engineering Technology Research Center, College of Animal Science and Technology, Nanjing Agricultural University, Nanjing, China

<sup>b</sup>Laboratory of Gastrointestinal Microbiology, Jiangsu Key Laboratory of Gastrointestinal Nutrition and Animal Health, National Center for International Research on Animal Gut Nutrition, College of Animal Science and Technology, Nanjing Agricultural University, Nanjing, China

**ABSTRACT** Subacute ruminal acidosis (SARA) is a major metabolic disease in lactating dairy cows caused by the excessive intake of high-concentrate diets. Here, we investigated the synergistic responses of rumen bacteria and epithelium to high-grain (HG)-induced SARA. Eight ruminally cannulated lactating Holstein cows were randomly assigned to 2 groups for a 3-week experiment and fed either a conventional (CON) diet or an HG diet. The results showed that the HG-feeding cows had a thickened rumen epithelial papilla with edge injury and a decreased plasma  $\beta$ -hydroxybutyrate concentration. The 16S rRNA gene sequencing results demonstrated that HG feeding caused changes in rumen bacterial structure and composition, which further altered rumen fermentation and metabolism. Cooccurrence network analysis revealed that the distribution of the diet-sensitive bacteria responded to the treatment (CON or HG) and that all diet-sensitive amplicon sequence variants showed low to medium degrees of cooccurrence. Metabolomics analysis indicated that the endothelial permeability-increasing factor prostaglandin E1 and the polyamine synthesis by-product 5'-methylthioadenosine were enriched under HG feeding. Transcriptome analysis suggested that cholesterol biosynthesis genes were upregulated in the rumen epithelium of HG cows. The gene expression changes, coupled with more substrate being available (total volatile fatty acids), may have caused an enrichment of intracellular cholesterol and its metabolites. All of these variations could coordinately stimulate cell proliferation, increase membrane permeability, and trigger epithelial inflammation, which eventually disrupts rumen homeostasis and negatively affects cow health.

**IMPORTANCE** Dairy cows are economically important livestock animals that supply milk for humans. The cow's rumen is a complex and symbiotic ecosystem composed of diverse microorganisms, which has evolved to digest high-fiber diets. In modern dairy production, SARA is a common health problem due to overfeeding of high-concentrate diets for an ever-increasing milk yield. Although extensive studies have been conducted on SARA, it remains unclear how HG feeding affects rumen cross talk homeostasis. Here, we identified structural and taxonomic fluctuation for the rumen bacterial community, an enrichment of certain detrimental metabolites in rumen fluid, and a general upregulation of cholesterol biosynthesis genes in the rumen epithelium of HG-feeding cows by multi-omics analysis. Based on these results, we propose a speculation to explain cellular events of coordinated rumen bacterial and epithelial adaptation to HG diets. Our work provides new insights into the exploitation of molecular regulation strategies to treat and prevent SARA.

**KEYWORDS** bacterial cooccurrence, cholesterol biosynthesis, high-grain diet, network analysis, rumen bacteria and epithelium, rumen metabolome

**Editor** Suzanne Lynn Ishaq, University of Maine

**Copyright** © 2022 Mu et al. This is an open-access article distributed under the terms of the [Creative Commons Attribution 4.0 International license](https://creativecommons.org/licenses/by/4.0/).

Address correspondence to Shengyong Mao, maoshengyong@njau.edu.cn.

The authors declare no conflict of interest.

**Received** 20 December 2021

**Accepted** 5 January 2022

**Published** 25 January 2022

For ruminants, the diverse and symbiotic microbial community of the rumen enables its multiple metabolic functions, which are associated with animal performance and the health traits of the host (1). The rumen microbial community is evolutionarily adapted to digest and metabolize high-fiber herbivore diets. Nevertheless, in modern dairy production, cows are often fed diets containing higher proportions of concentrates or other highly fermentable carbohydrates in pursuit of ever-increasing milk production, which conversely brings about rumen microbiota dysbiosis (2, 3). The dysbiosis of the rumen microbiota could further result in rumen fermentation alterations and, subsequently, metabolic disorders, which impair cow health and, ultimately, farm profitability (4, 5).

A common metabolic disorder caused by high-concentrate feeding in dairy cows is ruminal acidosis, which can be classified as acute ruminal acidosis and subacute ruminal acidosis (SARA) according to clinical manifestations (6). Acute ruminal acidosis is characterized by prolonged exposure to a ruminal pH of  $\leq 5.0$  and a decrease in blood pH bicarbonate, which is triggered by the overproduction of ruminal D-lactic acid. In contrast, SARA has no clinical manifestations, and the ruminal pH drops to values of around 5.5 (7). Despite this, SARA appears to be more prevalent and has become a major concern within the dairy industry (8).

In recent years, the evolution of sequencing technologies has enriched the study of SARA and expanded our understanding of it. Generally, these studies reveal alterations in the structure and function of the rumen microbiota during SARA, including reduced bacterial richness and diversity, elevated levels of propionate and total volatile fatty acids (VFAs), a decreased relative abundance of fibrolytic bacteria, depressed fiber degradation, an increased amount of amylolytic bacteria, and enhanced degradation of starch (3, 9, 10). In addition, SARA challenge promotes the accumulation of various deleterious compounds such as biogenic amines and bacterial lipopolysaccharide (11, 12). Also, the structural integrity and function of the rumen epithelium are compromised during SARA, which might affect host metabolism and activate local and systemic inflammation (13, 14). Nevertheless, systematic research, from adjustments in the rumen microbiota to changes in the rumen epithelium and host metabolism, for exploring the potential coordinated responses of the rumen microbiome profile and the host to SARA challenge is rather scarce.

Therefore, the objective of our study is to investigate the microbiome-host interaction that occurs during SARA by 16S rRNA gene sequencing, liquid chromatography-mass spectrometry (LC-MS) metabolomics, and transcriptome sequencing analyses using a cow model induced by a high-grain (HG) diet. This study expands our knowledge regarding the molecular mechanisms of the cross talk between the ruminal bacterial community and the host under high-concentrate diets and will be helpful for exploiting new molecular regulation strategies to attenuate the detrimental impact of SARA on ruminants.

## RESULTS

**Rumen pH and VFA profile.** The results for rumen pH and rumen fermentation parameters were reported previously (10). In brief, HG feeding resulted in an average duration of a rumen pH of  $< 5.8$  of 9.2 h/day without affecting the ruminal lactic acid concentration ( $P > 0.05$ ), indicating the successful induction of SARA with the HG treatment. Compared to the conventional (CON) diet group, HG feeding decreased the average daily pH, the acetate concentration, the acetate ratio, and the acetate/propionate ratio ( $P < 0.05$ ), whereas it increased the concentration of total VFAs, the concentration of propionate, the propionate ratio, and the concentration of valerate ( $P < 0.05$ ). The sampling day affected the rumen pH and all of the VFA levels ( $P < 0.05$ ). The interaction between diet and day affected the rumen pH; the levels of total VFAs, acetate, propionate, and butyrate; the acetate ratio; and the propionate ratio ( $P < 0.05$ ).

**Morphological parameters of rumen epithelial papillae.** The rumen epithelial papillae became darkened and thickened, with the appearance of edge injury, under HG feeding (Fig. 1A). Microscopic examination of the papillae revealed increases or a



**FIG 1** A high-grain (HG) diet affects the morphological parameters of rumen epithelial papillae. A representative visual graph (A) and light micrographs (B) of ruminal epithelial papillae in cows fed the conventional (CON) and HG diets are shown.

trend toward increases in the thicknesses of the stratum corneum (23.09 versus 8.36 mm [ $P < 0.001$ ]), granulosa (18.66 versus 10.13 mm [ $P = 0.001$ ]), and spinosum/basale (105.24 versus 80.60 mm [ $P = 0.054$ ]) layers as well as the total depth of the epithelium (147.00 versus 99.09 mm [ $P = 0.011$ ]) for the HG cows (Fig. 1B and Table 1). It also showed obvious effects of sampling day on the thicknesses of the stratum spinosum/basale and total epithelium layers ( $P < 0.05$ ). An interaction between diet and day was detected for stratum corneum thickness ( $P < 0.001$ ) (Table 1).

**Blood biochemical parameters.** The HG cows had a significantly lower plasma  $\beta$ -hydroxybutyrate (BHBA) concentration than the CON cows (0.39 versus 0.44 mmol/L [ $P = 0.009$ ]), and a diet-week interaction was also observed for it ( $P < 0.001$ ). But the day of sampling showed no apparent effects on any of the determined plasma constituents ( $P > 0.05$ ) (Table 1).

**Effects of HG feeding on rumen bacterial structure and composition.** All 1,264,737 sequences derived from 24 samples were generated through 16S rRNA gene sequencing. A total of 1,205,373 (95%) sequences passed the quality control, with an average number of 50,224 per sample. In total, 5,512 amplicon sequence variants (ASVs) were identified across all the rarefied samples, which were affiliated with 246 genera and 19 phyla.

Compared with the CON group, HG feeding significantly reduced the number of observed ASVs ( $P = 0.008$ ) and the Chao1 ( $P = 0.008$ ) and Shannon ( $P = 0.008$ ) indices but increased the Simpson index ( $P = 0.016$ ) (see Table S1A in the supplemental material), indicating decreased bacterial richness and evenness in the HG group. The principal-coordinate analysis (PCoA) results revealed obvious discrimination in the bacterial composition between the two groups ( $P = 0.001$  by permutational multivariate analysis of variance [PERMANOVA]) (Fig. S1).

**TABLE 1** Comparisons of ruminal epithelium thicknesses and blood biochemical parameters in cows fed the conventional diet and the high-grain diet<sup>a</sup>

Parameter	Value			P value		
	Mean for diet group		SEM	Diet	Day	Diet-day interaction
	CON	HG				
Ruminal epithelium thickness ( $\mu\text{m}$ )						
Total epithelium	99.09	147.00	2.59	0.011	0.023	0.066
Stratum corneum	8.36	23.09	0.49	<0.001	0.252	<0.001
Stratum granulosa	10.13	18.66	0.31	0.001	0.219	0.255
Stratum spinosum/basale	80.60	105.24	2.13	0.054	0.021	0.223
Blood biochemical parameters (concn)						
Glucose (mmol/L)	6.54	7.20	0.25	0.171	0.071	0.777
NEFAs ( $\mu\text{mol/L}$ )	155.70	153.13	4.41	0.793	0.682	0.779
Triglyceride (mmol/L)	1.30	1.55	0.07	0.066	0.125	0.386
Cholesterol (mmol/L)	5.38	5.33	0.18	0.893	0.870	0.659
BHBA (mmol/L)	0.44	0.39	0.02	0.009	0.086	<0.001

<sup>a</sup>CON, conventional; HG, high grain; NEFAs, nonesterified fatty acids; BHBA,  $\beta$ -hydroxybutyrate.

**TABLE 2** Comparison of rumen bacterial compositions between the conventional and high-grain diet groups at the genus level<sup>a</sup>

Taxon	Composition (%)			Q value		
	Mean for diet group			Diet	Day	Diet-day interaction
	CON	HG	SEM			
<i>Prevotella</i>	28.32	21.76	1.79	0.197	0.949	0.967
<i>Rikenellaceae</i> RC9 gut group	7.10	3.48	0.51	<0.001	0.840	0.982
Unclassified F082	5.60	4.08	0.45	0.367	0.770	0.982
Unclassified <i>Muribaculaceae</i>	5.09	7.15	0.54	0.169	0.881	0.967
<i>Succinivibrionaceae</i> UCG-002	4.04	1.69	0.44	0.048	0.924	0.987
<i>Succiniclasticum</i>	3.94	4.33	0.52	0.800	0.942	0.967
<i>Prevotellaceae</i> UCG-001	3.21	2.01	0.30	0.188	0.955	0.994
<i>Prevotellaceae</i> UCG-003	2.70	0.95	0.29	0.010	0.988	0.994
<i>Treponema</i>	2.57	0.87	0.33	0.048	0.994	0.994
<i>Oscillospiraceae</i> UCG-005	2.33	1.88	0.24	0.291	0.958	0.987
Unclassified <i>Clostridia</i> UCG-014	2.19	3.07	0.29	0.428	0.931	0.967
<i>Ruminococcus</i>	2.05	2.69	0.27	0.400	0.830	0.999
Unclassified p-251-o5	1.90	0.40	0.20	<0.001	0.994	0.999
NK4A214 group	1.75	1.30	0.18	0.122	0.770	0.987
<i>Christensenellaceae</i> R-7 group	1.63	0.70	0.15	0.010	0.994	0.994
Unclassified <i>Bacteroidales</i> RF16 group	1.62	1.46	0.18	0.962	0.770	0.987
<i>Fibrobacter</i>	1.17	0.53	0.11	0.041	0.994	0.987
<i>Oscillospiraceae</i> UCG-002	1.12	0.63	0.11	0.154	0.770	0.967
<i>Prevotellaceae</i> UCG-004	1.00	0.66	0.09	0.255	0.958	0.999
<i>Succinivibrionaceae</i> UCG-001	0.44	11.32	1.57	<0.001	0.994	0.987
Unclassified <i>Lachnospiraceae</i>	0.28	1.48	0.23	<0.001	0.994	0.999
<i>Shuttleworthia</i>	0.07	1.03	0.15	<0.001	0.994	0.987
<i>Prevotella_7</i>	0.01	6.88	1.55	0.010	0.994	0.987
<i>Dialister</i>	0.00	1.48	0.33	0.071	0.994	0.999

<sup>a</sup>Q values represent the Benjamini-Hochberg-adjusted *P* values. CON, conventional; HG, high grain.

We observed distinctive bacterial characteristics between the CON and HG groups at the phylum and genus levels in the predominant taxa, whose relative abundances were >1% in at least one group. At the phylum level, 19 phyla were detected in total, and the predominant phyla were comprised of the *Bacteroidota*, *Firmicutes*, *Proteobacteria*, *Spirochaetota*, *Patescibacteria*, and *Fibrobacterota*. There was a higher proportion of *Proteobacteria* ( $Q < 0.001$ ) and lower proportions of *Bacteroidota* ( $Q = 0.027$ ), *Spirochaetota* ( $Q = 0.027$ ), and *Fibrobacterota* ( $Q = 0.027$ ) in the HG group than in the CON group (Table S1B). At the genus level, a total of 246 genera were identified, and 24 abundant genera demonstrated proportions of >1%. Among them, the relative abundances of *Succinivibrionaceae* UCG-001, unclassified *Lachnospiraceae*, *Shuttleworthia*, and *Prevotella\_7* were enriched, whereas the relative abundances of the *Rikenellaceae* RC9 gut group, *Succinivibrionaceae* UCG-002, *Prevotellaceae* UCG-003, *Treponema*, unclassified p-251-o5, the *Christensenellaceae* R-7 group, and *Fibrobacter* were decreased in the HG group ( $Q < 0.05$ ) (Table 2).

At the ASV level, ASVs with an average percentage of >0.1% made up 96% of the total ASVs. Therefore, to obtain a more convincing power, we used indicator species analysis and a likelihood ratio test to examine the ASVs sensitive to the high-grain diet effect. The results indicated that HG feeding resulted in 234 diet-sensitive ASVs (dsASVs) between the two groups ( $P < 0.05$ ), among which 155 dsASVs had lower relative abundances in the HG cows. Moreover, 34 dsASVs showed a mean relative abundance of >0.1%, and 28 of them showed higher levels in the HG cows (Table S1C).

**Effects of HG feeding on rumen bacterial cooccurrence patterns.** To further explore the changes in the ecological structure of bacterial communities caused by HG feeding, we next investigated the distribution patterns of the 234 dsASVs in the rumen bacterial cooccurrence network. The results showed that most of the dsASVs were

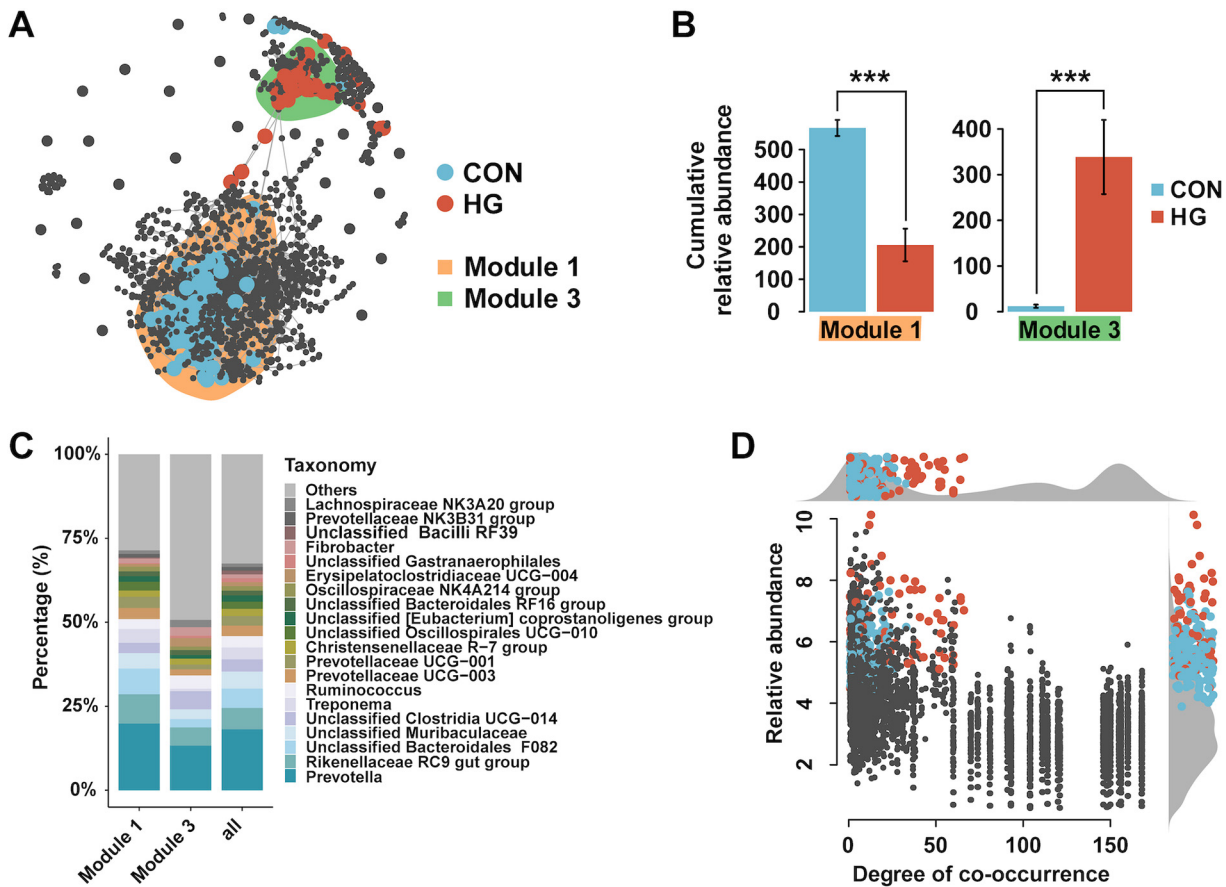


**FIG 2** Cooccurrence patterns of diet-sensitive amplicon sequence variants (dsASVs). (A) Cooccurrence network visualizing obvious positive correlations ( $r > 0.7$  and  $P < 0.001$ ) (shown with gray lines) between bacterial ASVs in the conventional (CON) and high-grain (HG) diet groups. Blue represents the dsASVs specific to the CON group, and red represents the dsASVs specific to the HG group. The ASVs that are unresponsive to either the CON or the HG group are displayed in gray. Shaded areas denote the modules that contained dsASVs in the top 10 most populated network modules. (B) Cumulative relative abundances (as counts per million [CPM] on the y axis [ $\times 1,000$ ]) of all ASVs in the 2 treatment (CON or HG)-sensitive modules. \*\*\*,  $P$  value of  $< 0.001$  by a Wilcoxon rank sum test. (C) Taxonomic composition of the 2 treatment (CON or HG)-sensitive modules at the genus level, compared to the total taxonomic distribution of the whole data set (column “all”). (D) Degree of cooccurrence of all ASVs in the cooccurrence network. Blue represents the dsASVs specific to the CON group, red represents the dsASVs specific to the HG group, and gray represents the ASVs that are unresponsive to either the CON or the HG group. Relative abundance is expressed as  $\log_{10}$ -transformed CPM.

primarily grouped into module 1 (M1) and module 3. Module 1 mainly involved dsASVs specific to the CON group, whereas dsASVs affiliated with the HG group were predominantly identified in module 3 (Fig. 2A). The cumulative relative abundances of all ASVs between the CON and HG groups in both module 1 and module 3 were obviously different ( $P < 0.001$  by a Wilcoxon rank sum test) (Fig. 2B). The phylogenetic distribution of the 2 modules was comparable to the taxonomic distribution of all ASVs, consisting of a taxonomically wide range of bacteria (Fig. 2C), which revealed that HG feeding does not target specific bacterial lineages. We determined the cooccurrence degrees for each node (number of connections to a node) and found that all dsASVs showed low to medium degrees of cooccurrence (Fig. 2D).

**Variations in rumen fluid metabolite profiles by HG feeding.** Totals of 144 and 120 metabolites were identified in the positive- and negative-ion modes, respectively. The principal-component analysis (PCA) results revealed a trend of a difference in metabolic profiles between the CON and HG groups ( $P < 0.1$  by PERMANOVA) (Fig. S2A and B). In the positive-ion mode of the partial least-squares discriminant analysis (PLS-DA) score plot,  $R^2Y$  was 0.902 and  $Q^2$  was 0.232; in the negative-ion mode,  $R^2Y$  was 0.848 and  $Q^2$  was 0.060. Although the  $Q^2$  values were low, the high  $R^2Y$  values indicated proper goodness of fit, and the PLS-DA results showed clear separations

**TABLE 3** Differential metabolites identified between the conventional and high-grain diet groups

Metabolite	VIP score <sup>a</sup>	Fold change <sup>b</sup>	P value
L-Ascorbic acid	1.33	9.27	0.050
PGE1	1.24	4.41	0.033
MG(12:0/0:0/0:0)	1.29	2.69	0.038
Adenine	1.84	1.98	0.005
2-Hydroxyvaleric acid	1.63	1.91	0.043
3-Hydroxysebacic acid	1.58	1.89	0.038
5'-Methylthioadenosine	1.57	1.80	0.015
Deoxyribose	1.61	1.69	0.038
LysoPA(8:0/0:0)	1.65	1.68	0.038
Hippuric acid	1.12	1.52	0.038
Palmitoleic acid	1.65	1.43	0.038
Phosphorylcholine	1.09	1.39	0.043
L-Isoleucine	1.22	0.82	0.038
3-Hydroxytetradecanedioic acid	1.66	0.82	0.033
Propenylcarnitine	1.57	0.82	0.050
2-Octenoic acid	1.45	0.81	0.050
Sebacic acid	1.58	0.80	0.028
Suberic acid	2.06	0.77	0.015
Undecanedioic acid	2.15	0.76	0.008
Hexanoylglycine	1.49	0.74	0.050
LysoPE(0:0/16:0)	1.55	0.71	0.043
L-Acetylcarnitine	1.81	0.69	0.015
1,11-Undecanedicarboxylic acid	2.13	0.68	0.009
Leukotriene E4	1.76	0.66	0.021
3-Hexenoic acid	1.89	0.65	0.011
3'-AMP	1.79	0.65	0.018
Benzoic acid	2.03	0.61	0.018
4-Hydroxyhippuric acid	1.77	0.61	0.021
$\alpha$ -Tocotrienol	1.76	0.59	0.050
2'-Deoxyuridine	2.04	0.59	0.015
Spermidine	2.03	0.58	0.009
LysoPC(16:0)	1.52	0.57	0.033
$\gamma$ -Tocotrienol	2.12	0.56	0.007
Choline	1.90	0.53	0.004
3-Hydroxyanthranilic acid	1.14	0.48	0.024
Homogentisic acid	1.41	0.45	0.015
LysoPE(0:0/18:0)	1.61	0.45	0.013
N-Acetyl-L-tyrosine	2.28	0.42	0.005
Cyclic AMP	2.73	0.41	0.000

<sup>a</sup>VIP, variable importance in projection.

<sup>b</sup>The fold change is calculated as the average level in the HG group relative to that in the CON group.

between the 2 groups (Fig. S2C and D). The low  $Q^2$  values might be attributed to the large samples and uncontrollable individual differences. The  $Q^2$  intercept values were less than 0.05, signifying that there was no overfitting (Fig. S2E and F).

Based on the criteria of a variable importance in projection (VIP) score of  $>1$  and a  $P$  value of  $<0.05$ , we obtained 39 differential metabolites in the positive- and negative-ion modes in total. Of these, the levels of 12 metabolites [L-ascorbic acid, prostaglandin E1 (PGE1), MG(12:0/0:0/0:0), adenine, 2-hydroxyvaleric acid, 3-hydroxysebacic acid, 5'-methylthioadenosine, deoxyribose, lysoPA(8:0/0:0), hippuric acid, palmitoleic acid, and phosphorylcholine] increased, whereas the levels of the other 27 metabolites decreased in the HG group with respect to the CON group (Table 3).

#### Effects on transcriptional profiles of rumen epithelial papillae by HG feeding.

Transcriptome sequencing of 24 rumen epithelial papilla samples generated a total of 810,033,258 high-quality paired reads, with an average number of 33,751,385 reads per sample. The PCA results showed that the transcriptional profiles of the CON and HG cows were clearly separated ( $P = 0.041$ ) (Fig. S3). We identified 596 differentially

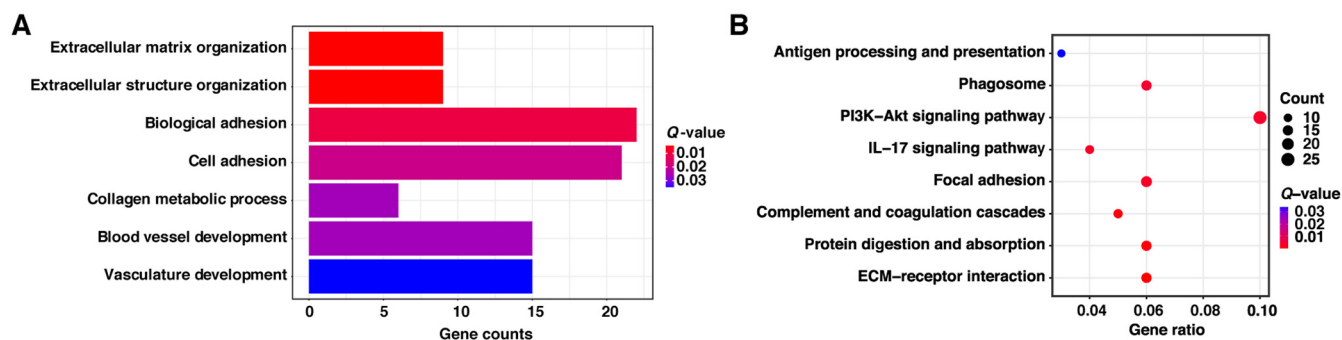


**FIG 3** Functional enrichment analysis of differentially expressed genes (DEGs) in rumen epithelial papillae between the conventional and high-grain diet groups. (A) The significantly enriched Gene Ontology biological process terms of DEGs. (B) The significantly enriched KEGG pathways of DEGs. Q values represent the Benjamini-Hochberg-adjusted  $P$  values.

expressed genes (DEGs) between the 2 groups in total, including 344 upregulated and 252 downregulated genes with HG feeding.

The results of the Gene Ontology (GO) enrichment of biological processes indicated that the DEGs were significantly enriched in 7 differential terms of extracellular matrix (ECM) organization, extracellular structure organization, biological adhesion, cell adhesion, collagen metabolic process, blood vessel development, and vasculature development ( $Q < 0.05$ ) (Fig. 3A). Moreover, almost all DEGs corresponding to these terms were upregulated in the HG group (Fig. S4A). The KEGG analysis showed that the DEGs were significantly enriched in 8 pathways, including ECM-receptor interaction, protein digestion and absorption, complement and coagulation cascades, focal adhesion, the interleukin-17 (IL-17) signaling pathway, the phosphatidylinositol 3-kinase (PI3K)–Akt signaling pathway, the phagosome, and antigen processing and presentation ( $Q < 0.05$ ) (Fig. 3B). Except for the IL-17 signaling pathway, DEGs related to the other 7 pathways were basically all upregulated in the HG group (Fig. S4B). With a visual plot of the IL-17 signaling pathway, we found that the associated DEGs were primarily involved in IL-17F-dependent signaling (Fig. S5), which exhibited a regulatory role in autoimmune disorders (15).

**Weighted gene coexpression network analysis of the correlation of the host transcriptome with rumen fermentation parameters, rumen epithelial papilla morphological parameters, and blood biochemical parameters.** For a comprehensive understanding of rumen epithelial transcriptome profiles under HG feeding, we further performed weighted gene coexpression network analysis (WGCNA) to identify the coexpressed gene modules that were highly correlated with host phenotypic traits. A total of 16 gene modules (M1 to M16) from all 14,078 host genes expressed in 24 samples were identified, among which M4 presented the most significant correlation (Fig. 4A). Generally, M4 was positively correlated with concentrations of propionate, valerate, and total VFAs; the propionate ratio; and ruminal epithelium thickness but was negatively correlated with the acetate concentration, the acetate/propionate ratio, the acetate ratio, and the plasma BHBA concentration ( $P < 0.05$ ) (Fig. 4A). The genes in M4 were apparently enriched in 36 GO biological process terms and 25 KEGG pathways, and almost all concerned genes were upregulated in the HG group (Fig. S6A and B). These GO terms were primarily associated with the RNA metabolic process and cholesterol biosynthetic process (Fig. 4B), while the KEGG pathways were mainly related to RNA transcription, protein synthesis, the metabolism of some amino acids and organic acids, the tricarboxylic acid cycle, RNA degradation, the proteasome, and steroid biosynthesis (Fig. 4C).

**Enhanced cholesterol biosynthesis in rumen epithelium by HG feeding.** Based on the strong correlation between the host transcriptome and rumen fermentation parameters suggested by WGCNA, we next explored the changes of VFA metabolism in the rumen epithelium around the genes in M4. After being absorbed by rumen epithelial cells, the VFAs were first transformed to acetyl-CoA under the actions of a cascade

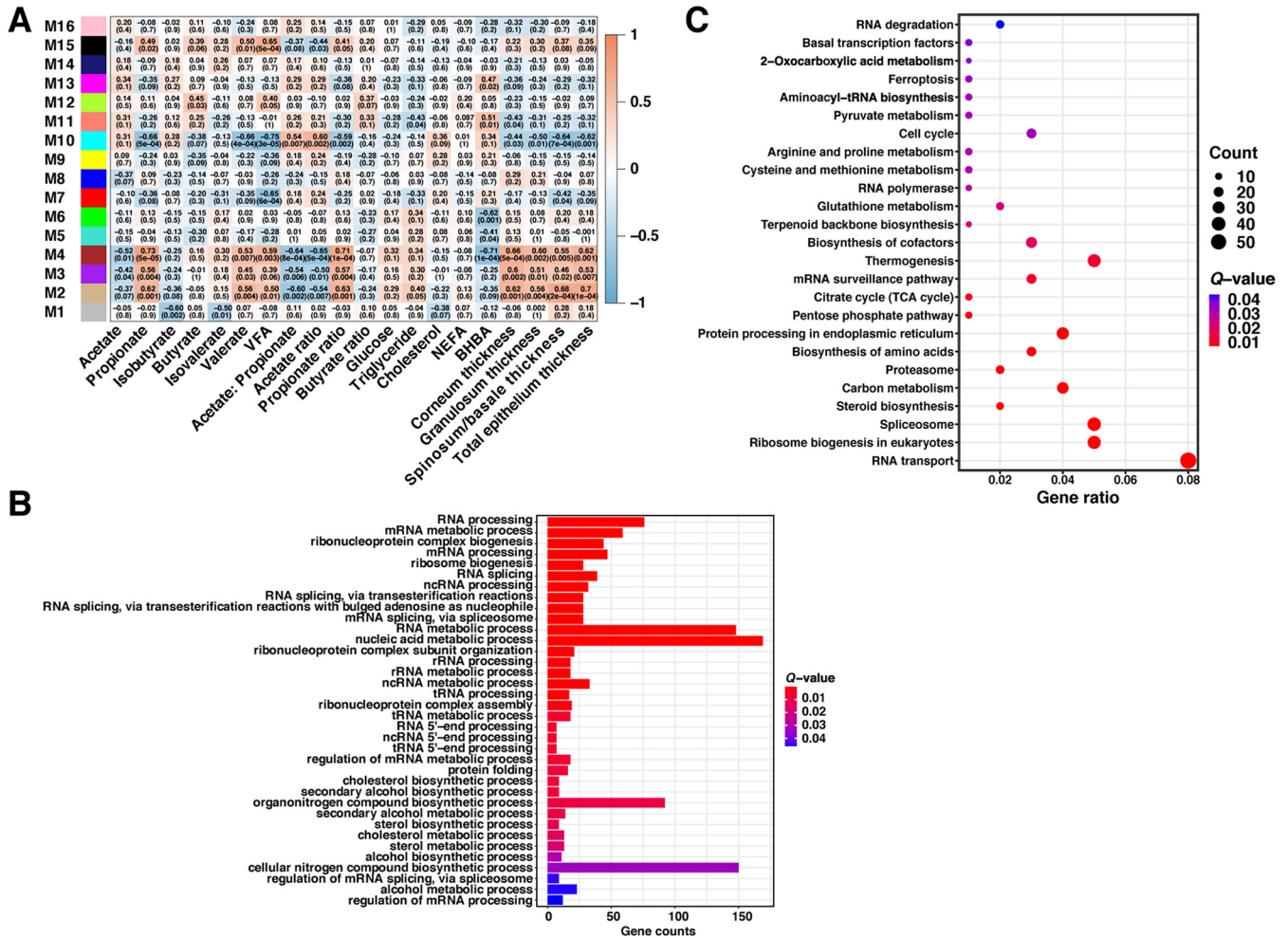


**FIG 4** Weighted gene coexpression network analysis of the correlation of the host transcriptome with host phenotypic traits. (A) The module-trait associations. Each row corresponds to a module eigengene, with a column for each trait. Numbers in the cells indicate the correlation coefficient and *P* value; red represents a positive correlation, and blue represents a negative correlation. (B) The significantly enriched Gene Ontology biological process terms in the M4 module. ncRNA, noncoding RNA. (C) The significantly enriched KEGG pathways in the M4 module. *Q* values represent the Benjamini-Hochberg-adjusted *P* values. TCA, tricarboxylic acid.

of enzymes; acetyl-CoA could then further proceed to ketogenesis or cholesterol biosynthesis via different metabolic pathways. Regarding cholesterol biosynthesis, most of the genes involved in this pathway were detected in M4, and they all had higher expression levels in the HG group, including one DEG (*FDFT1*) (Fig. 5A). For the ketogenesis pathway, there were not any genes concerning ketogenesis in mitochondria identified in M4 (Fig. 5B). Moreover, none of these ketogenic genes were DEGs (*Q* > 0.05) (Table S2). In brief, HG feeding promoted cholesterol biosynthesis without affecting ketogenesis in rumen epithelial cells in lactating dairy cows.

**DISCUSSION**

In the present study, we examined the coordinated adaptive variations between rumen bacteria, rumen fluid metabolomics, and transcriptome profiling of rumen epithelial papillae. It is important to emphasize that we primarily discuss the diet effect here due to our research focus and space constraints, although the effects of sampling day and diet-week interaction were also significant.

As broadly stated previously, our results characterized a typical shift in rumen fermentation and the rumen epithelium with SARA, including higher levels of propionate and total VFAs (3, 16), a reduced level of acetate (17, 18), and a changed rumen



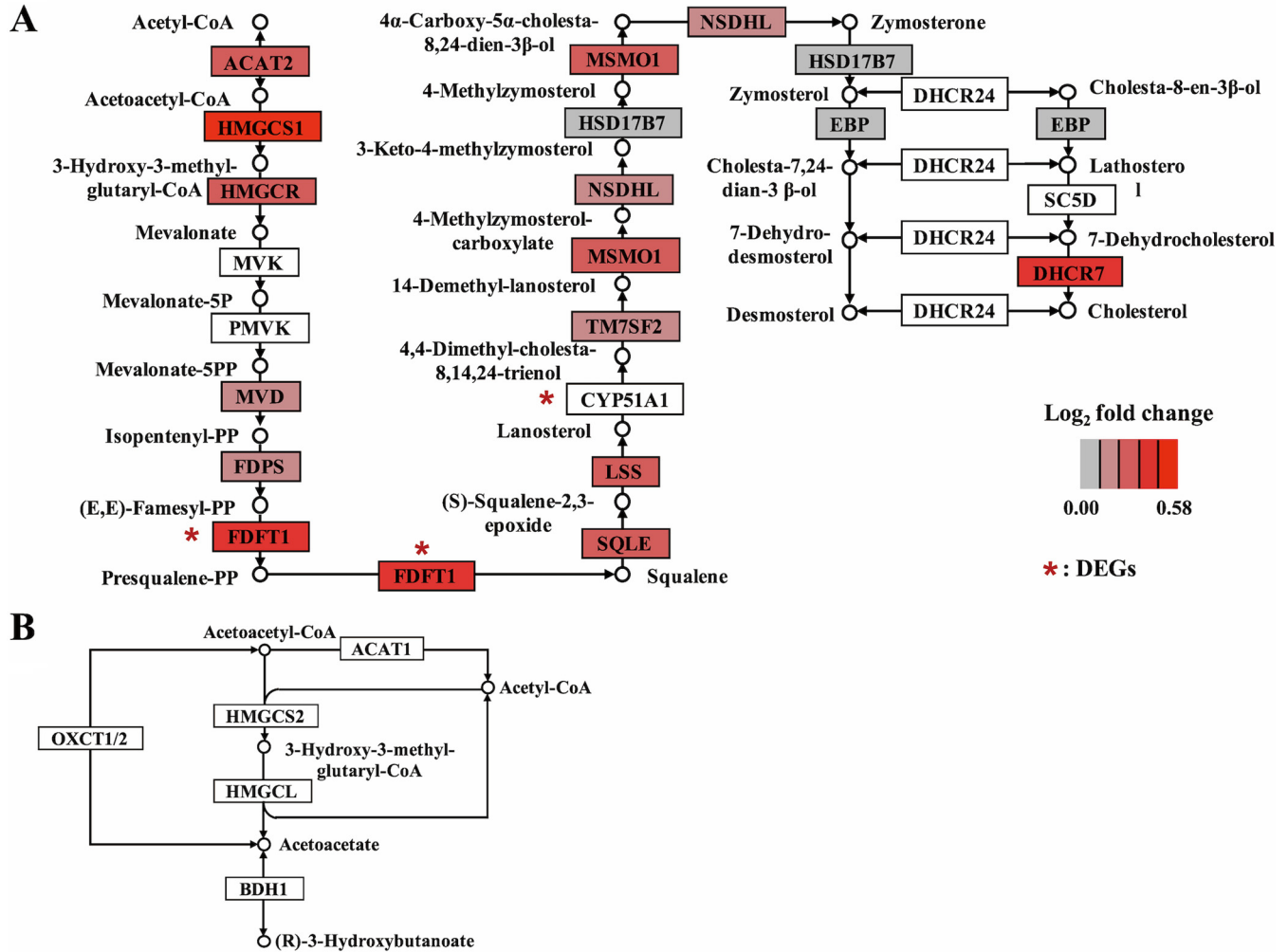


**FIG 5** Schematic overview of ketogenesis or cholesterol biosynthesis from acetyl-CoA in rumen epithelium cells. Gene expression patterns for the cholesterol biosynthesis pathway (A) and the ketogenesis pathway (B) were compared between the conventional (CON) and high-grain (HG) diet groups. The fold change is calculated as the average level in the HG group with respect to that in the CON group. Genes with a white background indicate that the gene is not detected in the M4 module. DEGs, differentially expressed genes.

epithelial morphology with tissue lesions (19–21). Additionally, we found an apparently decreased plasma BHBA concentration in the HG cows, which was also reported by some other researchers (22, 23).

The role of diverse microbes is the most decisive in rumen health and function. Here, we observed increased proportions of *Succinivibrionaceae* UCG-001, unclassified *Lachnospiraceae*, *Shuttleworthia*, and *Prevotella\_7* but decreased proportions of the *Rikenellaceae* RC9 gut group, *Succinivibrionaceae* UCG-002, *Prevotellaceae* UCG-003, *Treponema*, unclassified p-251-o5, the *Christensenellaceae* R-7 group, and *Fibrobacter* under HG feeding. Among them, the unclassified *Lachnospiraceae* and *Shuttleworthia* are members of starch-fermenting bacteria (2, 24), whereas *Treponema* and *Fibrobacter* are reported to be engaged in fiber degradation (25, 26). The enrichment of starch-degrading bacteria and the decreased abundance of fiber-degrading bacteria have been broadly documented in studies on SARA (9, 27); these eventually led to alterations in rumen fermentation, such as a decreased acetate level and elevated levels of propionate and total VFAs (8), which we also observed in our results. *Succinivibrionaceae* UCG-001 and *Succinivibrionaceae* UCG-002 belong to the *Succinivibrionaceae* family. Previous studies noted that *Succinivibrionaceae* UCG-001 contributed to the production of succinate (28), whereas *Succinivibrionaceae* UCG-002 was reported to be correlated with ruminal fatty acid metabolism (29). *Prevotella\_7* and *Prevotellaceae* UCG-003 belong to the

*Prevotellaceae* family, within which the dominant genus *Prevotella* had been reported to represent a group of bacteria that are capable of digesting various substrates (28). As for the *Rikenellaceae* RC9 gut group, the *Rikenellaceae* family itself is a relatively new taxonomic classification, and there is a great need for more data on its metabolic function, although Su et al. proposed one acetate-producing isolate from the *Rikenellaceae* family (30). Family p-251-o5 is a “*Candidatus*” taxon with no cultured representative as of yet. The *Christensenellaceae* R-7 group is most closely related to the species *Christensenella minuta* (31), which can produce acetate and butyrate from glucose (32). Altogether, these results demonstrated the possibility of disturbed rumen digestion and metabolism abilities in the HG cows and explained the altered rumen fermentation parameters.

The gut microbial ecosystem is a complex and dynamic community, and it allows a collective response to various perturbations, such as environment, diet, and health, which might further affect intestinal homeostasis and metabolism (33, 34). In our study, we found that the dsASVs specific to different groups clustered into distinct modules (Fig. 2A and B), indicating treatment-specific (HG or CON) responses of the bacterial community to HG feeding. Bacterial taxa that extensively interact with other taxa in the cooccurrence network are probably core members and are believed to play a key role within the microbiome (35). Our data showed that HG feeding is primarily limited to affecting ASVs with low to medium degrees of cooccurrence despite having an obvious ( $P = 0.001$ ) influence on community  $\beta$ -diversity (see Fig. S1 in the supplemental material). This finding suggests that although HG feeding causes structure fluctuation of the rumen bacterial community to some extent, it does not impact rumen bacterial taxa with keystone functions, implying the inertia and resilience of the rumen microbiota of adult ruminants to cope with certain outside perturbations (36).

Alterations in the composition and community structure of rumen bacteria lead to parallel changes in rumen fluid metabolites. One of the most interesting observations from our study was the increased levels of PGE1 and 5'-methylthioadenosine under HG feeding. PGE1 is an endothelial permeability-increasing factor (37); 5'-methylthioadenosine is a by-product of polyamine synthesis, and its accumulation can become toxic (38); and their enrichment might induce increased rumen epithelium permeability. Another interesting finding was the decreased concentrations of some beneficial compounds for the HG cows, such as  $\alpha$ -tocotrienol,  $\gamma$ -tocotrienol, and choline.  $\alpha$ -Tocotrienol and  $\gamma$ -tocotrienol are two different isoforms of vitamin E, which is the principal lipophilic antioxidant (39). Spermidine has pleiotropic protective effects on the organisms, such as anti-inflammatory properties, antioxidant functions, and preservation of mitochondrial function (40). Sun et al. demonstrate that rumen-protected choline can effectively alleviate oxidative stress and improve the immune function of transition dairy cows (41). We also found decreased levels of some amino acids and their derivatives (L-isoleucine, hexanoylglycine, and N-acetyl-L-tyrosine), suggesting that HG feeding affected protein digestion and metabolism of the cows. Besides, our data revealed a cluster of differential metabolites that are degradation products of the rumen microbiota (adenine, 5'-methylthioadenosine, 2'-deoxyuridine, and 3'-AMP) between the 2 groups; this indicated the cell lysis of certain microbiota members that could not survive the low-pH stress, which was consistent with previously noted findings on SARA (42, 43).

Accumulating evidence shows that changes in the structure and function of the intestinal microbiota affect host metabolism and immunity, especially for the luminal epithelium (44, 45). In ruminants, previous studies revealed that HG diet feeding caused an accelerated cell cycle, a promotion of cell proliferation, and a local inflammatory response of the rumen epithelium (20, 21). In this study, the results for the rumen epithelial transcriptome demonstrated that the DEGs were significantly enriched in the GO biological processes of cellular processes (extracellular matrix organization, extracellular structure organization, and cell adhesion) and system development (blood vessel development and vasculature development) as well as the KEGG pathway of signaling molecules and interaction (ECM-receptor interaction and the PI3K-Akt signaling

pathway), the immune system (complement and coagulation cascades and antigen processing and presentation), and cellular processes (focal adhesion and the phagosome). Meanwhile, almost all corresponding DEGs were upregulated in the HG group. Taken together, we speculate that these enrichments mirror the improved cell cycle-regulating adaptation to maximize the absorptive surface area for increasing nutrient loads and an immune defense response of the rumen epithelium to HG feeding. This speculation corresponds to the morphological observations of rumen epithelial papillae (Fig. 1), which indicated thickening and edge injury visible to the naked eye, and microscopically enhanced ruminal epithelium thickness under HG feeding.

Further WGCNA indicated that the M4 module showed the most significant correlation with rumen fermentation parameters, ruminal epithelium thickness, and the plasma BHBA concentration. Moreover, the markedly enriched functions of the M4 module were mainly concentrated on RNA metabolic processes, protein synthesis, the metabolism of some amino acids and organic acids, the tricarboxylic acid cycle, RNA degradation, the proteasome, and steroid biosynthesis (Fig. 4B and C), with almost all corresponding genes being upregulated in the HG group. Except for steroid biosynthesis, the enrichment of these functions might also imply an accelerated cell cycle and an inflammatory event in rumen epithelial cells (46, 47), which is in agreement with the above-described enrichment results for DEGs.

In this study, the rumen VFA concentration was elevated during HG feeding; this elevation might stimulate the absorption of rumen epithelial cells (48) and promote their metabolism. VFA metabolism in the rumen epithelium predominantly includes pathways of ketogenesis and cholesterol synthesis (49). Ketogenesis in the rumen epithelium proceeds exclusively in mitochondria (14), whereas cholesterol synthesis proceeds in the cytoplasm and endoplasmic reticulum (50). Cholesterol is an essential component of mammalian cell membranes, but the excessive accumulation of cellular cholesterol and its metabolites can trigger an inflammatory response, cell proliferation, and oxidative stress and influence membrane permeability (14). In our study, we found a general upregulation of cholesterol biosynthesis genes in the rumen epithelium under HG feeding, and almost all of them were detected in M4. Collectively, the gene expression changes, in combination with more substrate being available, may have caused an enrichment of intracellular cholesterol, which could be related to well-documented symptoms of the rumen epithelium under HG diet feeding, such as an inflammation response, accelerated cell cycle, and increased membrane permeability (20, 21, 51). At the same time, it echoes the function enrichment results for the DEGs and the M4 module. However, these correlations are just our speculation and need further experimental verification in the future.

With regard to ketogenesis, we found that HG feeding did not affect the gene expression levels of ketogenic enzymes. Similarly, Steele et al. also reported the lack of differential expression of ketogenic enzyme genes using microarray analysis between cattle fed HG and those fed high-forage diets and validated this by quantitative PCR (qPCR) (14). For ruminants, acetate and ketone bodies are the main energetic substrates and can be converted to triglycerides in adipocytes and the mammary gland (52). Acetate release by the portal-drained viscera (PDV) was evidently decreased when the dietary concentrate level increased (53), which conversely would lead to a rise in the utilization of ketone bodies by peripheral tissues. Furthermore, a high metabolic cost of the rumen epithelium is expected during HG feeding owing to the stimulated VFA absorption, the accelerated outflow of rumen fluid (48), and other functional adaptations (the cell cycle and the inflammatory response). In the fed state, blood-circulating ketone bodies (acetone, acetoacetate, and BHBA) are mainly derived from synthesis by the rumen epithelium (54). The BHBA concentration is generally used as a reference for plasma ketone body levels (55). Considered altogether, it can be presumed that the decrease in the plasma BHBA concentration from our study is due to increased utilization by peripheral tissues rather than the differential gene expression levels of enzymes controlling ketogenesis in the rumen epithelium.

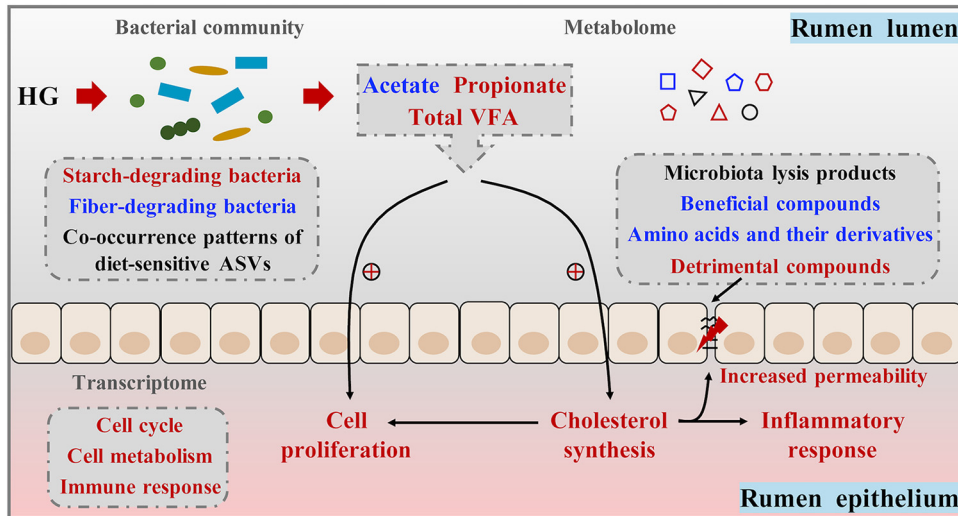


**FIG 6** Schematic overview of the coordinated responses of rumen bacteria and epithelium to high-grain (HG) diet feeding in lactating dairy cows. Red represents upregulated levels, and blue represents downregulated levels. The plus signs represent upregulated gene expression levels. ASV, amplicon sequence variant; VFA, volatile fatty acids.

In conclusion, our study demonstrated that HG feeding caused changes in rumen bacterial profiles (structure, composition, and cooccurrence patterns of dsASVs); these changes then altered rumen fermentation, including decreased acetate concentrations and increased concentrations of propionate and total VFAs. In parallel, some detrimental metabolites were enriched, which might have increased membrane permeability. The elevated total VFA level accelerated cell proliferation of the rumen epithelium to maximize its absorptive ability and upregulated the genes for cholesterol biosynthesis. The gene expression changes, combined with more substrate being available, may have caused an accumulation of intracellular cholesterol and its metabolites, which further stimulated cell proliferation, increased membrane permeability, and triggered epithelial inflammation (Fig. 6). Additionally, due to the decreased acetate release by PDV tissues during HG feeding, there was an augmented utilization of BHBA by peripheral tissues, which resulted in a reduced plasma BHBA concentration. These findings shed new light on the coordinated microbiota-host cross talk in disturbing host homeostasis under HG feeding in lactating dairy cows.

## MATERIALS AND METHODS

All the procedures in this experiment were conducted according to animal protection law based on the *Guide for the Care and Use of Laboratory Animals* (56) and approved by the Ethics Committee of Nanjing Agricultural University.

**Animals, diets, and experimental design.** Eight ruminally cannulated (internal diameter, 10 cm) multiparous and clinically healthy lactating Holstein cows (body weight of  $582 \pm 50$  kg;  $120 \pm 6$  days in milk; milk yield of  $18.2 \pm 2.66$  kg/day) were selected for the experiment. Feeding and management were described previously (10). Briefly, the animals were randomly assigned to two groups and housed in individual tie stalls during the 21-day trial period; one group was given a CON diet (40% concentrate [dry matter basis]), and the other group was given an HG diet (60% concentrate [dry matter basis]) (see Table S3 in the supplemental material). The diets were prepared as total mixed rations and formulated to meet or exceed NRC nutrient recommendations (57).

**Rumen pH measurement, rumen content sampling, and analysis.** Rumen pH was measured at 0 h before the morning feeding and 2, 4, 6, 8, and 12 h later on days 3, 6, 7, 13, 14, 20, and 21 with a mobile pH meter (HI 99161; Hanna Instruments). The rumen content samples were collected from the ventral sac of the rumen before morning feeding and 4, 8, 12 h later on days 7, 14, and 21 via the rumen fistula. After collection, the ruminal contents were divided into 3 aliquots, 1 of which was immediately placed into liquid nitrogen for microbial DNA extraction and the other 2 of which were strained through 4 layers of sterile cheesecloth to obtain rumen fluid and frozen in liquid nitrogen or at  $-20^{\circ}\text{C}$  separately for later rumen metabolome analysis and VFA quantification (10).

**Blood sampling and analysis.** Blood samples were collected via the tail vein into evacuated  $\text{K}_2\text{-EDTA}$  (anticoagulation) tubes 6 h after the morning feeding on days 7, 14, and 21. Plasma was separated by centrifugation at  $3,000 \times g$  for 15 min at  $4^{\circ}\text{C}$  and stored at  $-80^{\circ}\text{C}$  until analysis. The concentrations

of glucose, nonesterified fatty acids (NEFAs), triglyceride, cholesterol, and BHBA in plasma were determined in duplicate using standard procedures and commercial kits (Nanjing Jiancheng Biology Research Institute, Nanjing, China).

**Rumen epithelial papilla biopsies and microscopic study.** Rumen epithelial papillae were biopsied from the ventral sac before evening feed delivery on days 7, 14, and 21, as described previously (19). First, the reticulorumen contents were partially emptied to facilitate the retraction of the ventral sac to the fistula. Next, sterile surgical scissors were used to excise approximately 200 mg of rumen papillae, and the papillae were quickly rinsed several times in ice-cold phosphate-buffered saline to remove feed particles. After washing, papillae were stored in liquid nitrogen or 4% paraformaldehyde (PFA) for subsequent transcriptome analysis or morphological observation, respectively.

Five papillae per cow per time point were prepared for light microscopy histomorphometric analysis using methods described in a previous publication (58). PFA-fixed papillae were dehydrated, paraffin embedded, sectioned, and stained with hematoxylin and eosin before being mounted for analysis. Three images were captured per papilla, including the base, middle, and tip of the rumen papilla, and a total of 15 replicates were taken per time point per cow. Image Pro Plus software (Media Cybernetics, Bethesda, MD, USA) was used to measure the thickness of each stratum (corneum, granulosum, and spinosum/basale) at a magnification of  $\times 40$  according to previously defined criteria (19).

**Microbial DNA extraction, 16S rRNA gene sequencing, and analyses.** Genomic DNAs of the rumen content samples before the morning feeding on days 7, 14, and 21 were isolated using an EZNA stool DNA kit (Omega BioTek) according to the manufacturer's procedures, with a bead-beating step (BioSpec Products) added to break down the cell walls of the microbes. The concentration and quality of the extracted DNA were examined using a NanoDrop 1000 spectrophotometer (Nyxor Biotech, Paris, France) and 1.0% agarose gel electrophoresis, respectively. The V3-V4 region of the 16S rRNA gene was amplified using the 341 forward primer (5'-CCTAYGGGRBGCASCAG-3') and the 806 reverse primer (5'-GGACTACNNGGTATCTAAT-3') (59). A total of 27 cycles of PCR amplification were conducted. The PCR products were purified with the GeneJET gel extraction kit (Thermo Scientific). Amplicon libraries were constructed using a New England BioLabs (NEB) Next Ultra DNA library prep kit for Illumina and sequenced (paired end, 2 by 250 bp) on the Illumina MiSeq platform (Illumina Inc.).

The raw sequences were demultiplexed using an in-house Perl script based on their unique barcodes and processed to filter low-quality reads with the following criteria: the 250-bp reads were truncated at any site receiving an average quality score of  $< 20$  over a 10-bp sliding window, discarding the truncated reads that were shorter than 50 bp. Paired-end reads were then merged using FLASH v1.2.7 (60), with a minimum 10-bp overlap. The sequences were further screened to remove chimeras using Vsearch software (v2.18.0) (61), followed by dereplication and ASV feature table construction using the DADA2 (62) plug-in implemented in QIIME 2 v2021.08 (63). Taxonomy was assigned to ASVs using the naive Bayes classifier (64) trained against the SILVA v138 database (65) trimmed to match the V3-V4 region sequenced. To control for intersample depth variability, all samples were rarefied to 23,278 reads, the size of the smallest sample. Rarefaction curves were generated to ensure adequate sequencing depth (Fig. S7). The rarefied ASV count table was used for analyses of  $\alpha$ -diversity,  $\beta$ -diversity, and taxonomic classification.  $\alpha$ - and  $\beta$ -diversity metrics were calculated using the q2-diversity plug-in in QIIME 2.  $\beta$ -Diversity was assessed using Bray-Curtis dissimilarity and visualized by a PCoA plot. The statistical significance of the PCoA was determined using the adonis function in the R package vegan (v2.5-7) with 999 permutations.

**dsASV identification and bacterial cooccurrence network construction.** We employed indicator species analysis with the R package indicpecies (v1.7.9) and a likelihood ratio test with the R package edgeR (v3.32.1), which were more sensitive statistical tests than standard nonparametric tests (66), to identify the ASVs responsible for the high-grain diet effect. The ASV sequence counts were normalized using the "trimmed means of M" method and were expressed as relative abundance counts per million in advance (67). Only ASVs that were confirmed by both the indicator species analysis and the likelihood ratio test simultaneously were considered to have a significant difference between groups, and we defined those ASVs as dsASVs. Statistical significances were declared at  $P$  values of  $< 0.05$ .

The bacterial cooccurrence network was constructed using the R package igraph (v1.2.6) with the Fruchterman-Reingold layout with 9,999 permutations. Relationships between ASVs were tested with the Spearman rank correlation utilizing the normalized counts per million, and positive correlations ( $r > 0.7$  and  $P < 0.001$ ) were visualized. Network module identification was conducted using a fast-greedy modularity optimization procedure (68).

**Rumen metabolome analysis.** Twenty-four rumen fluid samples obtained before the morning feeding on days 7, 14, and 21 were slowly thawed at 4°C, and from each sample, a 100- $\mu$ L aliquot was taken to mix with 300  $\mu$ L of methanol and 10  $\mu$ L of the internal standard (2.8 mg/mL L-2-chlorophenylalanine). The mixture was vortexed for 30 s and maintained at  $-20^{\circ}\text{C}$  for 60 min, followed by centrifugation at  $13,800 \times g$  for 10 min at 4°C. The resulting supernatant was collected for analysis.

The LC-MS analysis was performed using an Ultimate 3000LC-Q-Exactive instrument (Thermo, CA, USA) incorporating a Hyper gold C<sub>18</sub> column (100 mm by 2.1 mm, 1.9  $\mu$ m; Thermo). The column temperature was maintained at 40°C. The mobile phase consisted of mobile phase A (water plus 5% [vol/vol] acetonitrile and 0.1% [vol/vol] formic acid) and mobile phase B (acetonitrile plus 0.1% [vol/vol] formic acid) at a flow rate of 0.3 mL/min. The elution procedure was as follows: 5% mobile phase B from 0 to 1 min, 5% to 95% mobile phase B from 1 to 11 min, and 95% to 5% mobile phase B from 11 to 19.5 min. The injection volume was 10  $\mu$ L, and the autosampler was maintained at 4°C. The mass spectrometric settings for positive/negative-ion modes were as follows: a heater temperature of 300°C, a sheath gas flow rate of 45 arb, an auxiliary gas flow rate of 15 arb, a sweep gas flow rate of 1 arb, a spray voltage of

3.0 kV/3.2 kV, a capillary temperature of 350°C, and an S-lens radio frequency (RF) level of 30%/60%, respectively.

The raw data were analyzed with feature extraction and preprocessing by Compound Discoverer 2.0 software (Thermo Scientific). Ion peak data that were present in <50% of the samples were removed. The main parameters were set as follows: an intensity threshold of 300,000, an  $m/z$  range of 70 to 1,050, an  $m/z$  width of 5 ppm, a frame time width of 0.2 min, and retention time start and end values of 0.01 and 19.5 min, respectively. Next, they were normalized according to the interior label and postedited in Excel 2010 software. The online Human Metabolome Database (<https://hmdb.ca>) and KEGG database (<https://www.genome.jp/kegg/>) were used to identify metabolites by aligning the molecular mass data. The metabolites were reported only when the difference between the theoretical mass and the observed mass was <20 ppm and further validated by isotopic distribution measurement. PCA, PLS-DA, and loading plots were carried out using SIMCA-P software (version 13.0; Umetrics, Umea, Sweden). The PLS-DA models were validated based on the variation interpretation ( $R^2Y$ ) and predictability ( $Q^2$ ) of the model in cross-validation and permutation tests with 200 iterations. Differential metabolites were identified according to the VIP obtained from the PLS-DA model and statistical analysis (VIP score of >1 and  $P$  value of <0.05). When the metabolites were identified in both positive- and negative-ion modes, the data in the mode with the lower  $P$  value were retained.

**Epithelial RNA extraction and sequencing.** Total RNA of rumen epithelial papillae from 24 samples obtained before evening feed delivery on days 7, 14, and 21 was extracted using TRIzol (TaKaRa Bio, Otsu, Japan). The RNA concentration was measured using a NanoDrop 1000 spectrophotometer (Thermo Fisher Scientific, Waltham, MA, USA). RNA quality was evaluated with an Agilent 2100 bioanalyzer (Agilent Technologies, San Diego, CA, USA), and the RNA integrity number was  $\geq 8.5$  for all samples. The sequencing libraries were prepared with 1  $\mu\text{g}$  of high-quality total RNA using an Illumina TruSeq RNA sample preparation kit (Illumina, San Diego, CA, USA) to enrich poly(A)-tailed host mRNA with oligo(dT) beads, and sample-specific barcodes were added. After quantification by a TBS 380 fluorometer (Turner Biosystems, Sunnyvale, CA, USA), the paired-end libraries (2 by 150 bp) were sequenced on the Illumina NovaSeq 6000 platform.

**Transcriptome analyses.** The raw sequences were filtered to remove adaptor contaminations and low-quality reads using Trimmomatic v0.36 (69). Next, clean reads were aligned to the *Bos taurus* reference genome ARS-UCD1.2 using HISAT2 with default parameters (70), and HTSeq v0.11.1 was used to count the reads mapped to each gene (71). Differential expression analyses were conducted with DESeq2 v1.30.1 (72). DEGs were screened with a cutoff condition of an absolute fold change of >1.2 and a Benjamini-Hochberg-adjusted  $P$  value ( $Q$ ) of <0.05.

The R package WGCNA v1.70-3 was employed to identify trait-related gene coexpression modules (73). Gene expression data were prefiltered by keeping genes with at least one read across all 24 samples and then normalized by transcripts per kilobase per million (TPM) and  $\log_2$  transformed [ $\log_2(\text{TPM} + 1)$ ]. We use the automatic one-step function `blockwiseModules` to perform network construction and module detection with the following parameters: power of 14, `maxBlockSize` of 15,000, `minModuleSize` of 30, signed network type, `mergeCutHeight` of 0.25, and default parameters for other settings. Because of the normal distribution of the data (Shapiro-Wilk test), module-trait relationships were calculated by Pearson correlation analysis.

Principal-component analysis was performed using the `prcomp` function of R (version 4.0.5). GO enrichment and KEGG analyses were implemented using the R package `clusterProfiler` v3.18.1 (74), and biological categories were considered significant at a  $Q$  value of <0.05.

**Statistical analyses.** The linear mixed-effects model (MIXED) procedure of IBM SPSS statistics V25.0 (IBM Corp., Armonk, NY, USA) was performed to assess the differences in rumen pH, VFAs, blood biochemical parameters, and ruminal epithelium thickness. The treatment (CON or HG), day, and their interaction were treated as fixed factors. The cow was considered a random effect, and the hour or replicates of rumen papillae were considered a repeated measure. Effects were deemed significant when the  $P$  value was <0.05.

The data on  $\alpha$ -diversity indices, relative abundances of bacterial communities, and the rumen fluid metabolome were analyzed using the nonparametric Scheirer-Ray-Hare extension of the Kruskal-Wallis test (75), which is a nonparametric analog of analysis of variance (ANOVA) based on ranked variates with two independent factors (group and day) plus their interactions. For rumen bacterial abundance, differences were regarded as being significant at a  $Q$  value of <0.05.

**Data availability.** Raw reads from rumen content 16S rRNA gene sequencing were deposited in the NCBI SRA database under accession number [PRJNA761857](https://www.ncbi.nlm.nih.gov/sra/PRJNA761857). Raw reads from rumen epithelium transcriptome sequencing were deposited in the NCBI SRA database under accession number [PRJNA762113](https://www.ncbi.nlm.nih.gov/sra/PRJNA762113). Metabolomics data were deposited in the CNSA (<https://db.cngb.org/cnsa/>) of the CNGbDb under accession number [CNP0002475](https://www.ncbi.nlm.nih.gov/sra/CNP0002475).

## SUPPLEMENTAL MATERIAL

Supplemental material is available online only.

**FIG S1**, PDF file, 0.03 MB.

**FIG S2**, PDF file, 0.3 MB.

**FIG S3**, PDF file, 0.01 MB.

**FIG S4**, PDF file, 0.05 MB.

**FIG S5**, PDF file, 0.3 MB.

**FIG S6**, PDF file, 0.1 MB.

**FIG S7**, PDF file, 0.04 MB.

**TABLE S1**, XLSX file, 0.02 MB.

**TABLE S2**, DOCX file, 0.05 MB.

**TABLE S3**, DOCX file, 0.05 MB.

## ACKNOWLEDGMENTS

This research was funded by the National Key R&D Program of China (2021YFF1000700) and the Fundamental Research Funds for the Central Universities (JCY201905; Beijing).

Our project was supported by the high-performance computing platform of the Bioinformatics Center, Nanjing Agricultural University. We also thank Shanghai Sensichip Infotech Co. Ltd., Shanghai, People's Republic of China.

We report no conflict of interest.

## REFERENCES

- Huws SA, Creevey CJ, Oyama LB, Mizrahi I, Denman SE, Popova M, Muñoz-Tamayo R, Forano E, Waters SM, Hess M, Tapio I, Smidt H, Krizsan SJ, Yáñez-Ruiz DR, Belanche A, Guan L, Gruninger RJ, McAllister TA, Newbold CJ, Roehe R, Dewhurst RJ, Snelling TJ, Watson M, Suen G, Hart EH, Kingston-Smith AH, Scollan ND, do Prado RM, Pilau EJ, Mantovani HC, Attwood GT, Edwards JE, McEwan NR, Morrisson S, Mayorga OL, Elliott C, Morgavi DP. 2018. Addressing global ruminant agricultural challenges through understanding the rumen microbiome: past, present, and future. *Front Microbiol* 9:2161. <https://doi.org/10.3389/fmicb.2018.02161>.
- Neubauer V, Petri R, Humer E, Kroger I, Mann E, Reisinger N, Wagner M, Zebeli Q. 2018. High-grain diets supplemented with phytogenic compounds or autolyzed yeast modulate ruminal bacterial community and fermentation in dry cows. *J Dairy Sci* 101:2335–2349. <https://doi.org/10.3168/jds.2017-13565>.
- Mao SY, Zhang RY, Wang DS, Zhu WY. 2013. Impact of subacute ruminal acidosis (SARA) adaptation on rumen microbiota in dairy cattle using pyrosequencing. *Anaerobe* 24:12–19. <https://doi.org/10.1016/j.anaerobe.2013.08.003>.
- Sutton JD, Dhanoa MS, Morant V, France J, Napper DJ, Schuller E. 2003. Rates of production of acetate, propionate, and butyrate in the rumen of lactating dairy cows given normal and low-roughage diets. *J Dairy Sci* 86:3620–3633. [https://doi.org/10.3168/jds.S0022-0302\(03\)73968-X](https://doi.org/10.3168/jds.S0022-0302(03)73968-X).
- Kleen JL, Cannizzo C. 2012. Incidence, prevalence and impact of SARA in dairy herds. *Anim Feed Sci Technol* 172:4–8. <https://doi.org/10.1016/j.anifeeds.2011.12.003>.
- Jaramillo-López E, Itza-Ortiz MF, Peraza-Mercado G, Carrera-Chávez JM. 2017. Ruminal acidosis: strategies for its control. *Austral J Vet Sci* 49:139–148. <https://doi.org/10.4067/S0719-81322017000300139>.
- Hernández J, Benedito JL, Abuelo A, Castillo C. 2014. Ruminal acidosis in feedlot: from aetiology to prevention. *ScientificWorldJournal* 2014:702572. <https://doi.org/10.1155/2014/702572>.
- Abdela N. 2016. Sub-acute ruminal acidosis (SARA) and its consequence in dairy cattle: a review of past and recent research at global prospective. *Achiev Life Sci* 10:187–196. <https://doi.org/10.1016/j.als.2016.11.006>.
- Mickdam E, Khiaosa-Ard R, Metzler-Zebeli BU, Klevenhusen F, Chizzola R, Zebeli Q. 2016. Rumen microbial abundance and fermentation profile during severe subacute ruminal acidosis and its modulation by plant derived alkaloids in vitro. *Anaerobe* 39:4–13. <https://doi.org/10.1016/j.anaerobe.2016.02.002>.
- Mu YY, Qi WP, Zhang T, Zhang JY, Mao SY. 2021. Gene function adjustment for carbohydrate metabolism and enrichment of rumen microbiota with antibiotic resistance genes during subacute rumen acidosis induced by a high-grain diet in lactating dairy cows. *J Dairy Sci* 104:2087–2105. <https://doi.org/10.3168/jds.2020-19118>.
- Humer E, Kröger I, Neubauer V, Schedle K, Reisinger N, Zebeli Q. 2018. Supplementing phytogenic compounds or autolyzed yeast modulates ruminal biogenic amines and plasma metabolome in dry cows experiencing subacute ruminal acidosis. *J Dairy Sci* 101:9559–9574. <https://doi.org/10.3168/jds.2018-14744>.
- Wang DS, Zhang RY, Zhu WY, Mao SY. 2013. Effects of subacute ruminal acidosis challenges on fermentation and biogenic amines in the rumen of dairy cows. *Livest Sci* 155:262–272. <https://doi.org/10.1016/j.livsci.2013.05.026>.
- Zebeli Q, Metzler-Zebeli BU. 2012. Interplay between rumen digestive disorders and diet-induced inflammation in dairy cattle. *Res Vet Sci* 93:1099–1108. <https://doi.org/10.1016/j.rvsc.2012.02.004>.
- Steele MA, Vandervoort G, AlZahal O, Hook SE, Matthews JC, McBride BW. 2011. Rumen epithelial adaptation to high-grain diets involves the coordinated regulation of genes involved in cholesterol homeostasis. *Physiol Genomics* 43:308–316. <https://doi.org/10.1152/physiolgenomics.00117.2010>.
- Patel DD, Kuchroo VK. 2015. Th17 cell pathway in human immunity: lessons from genetics and therapeutic interventions. *Immunity* 43:1040–1051. <https://doi.org/10.1016/j.immuni.2015.12.003>.
- Gozho GN, Krause DO, Plaizier JC. 2007. Ruminal lipopolysaccharide concentration and inflammatory response during grain-induced subacute ruminal acidosis in dairy cows. *J Dairy Sci* 90:856–866. [https://doi.org/10.3168/jds.S0022-0302\(07\)71569-2](https://doi.org/10.3168/jds.S0022-0302(07)71569-2).
- Pan XH, Yang L, Xue FG, Xin HR, Jiang LS, Xiong BH, Beckers Y. 2016. Relationship between thiamine and subacute ruminal acidosis induced by a high-grain diet in dairy cows. *J Dairy Sci* 99:8790–8801. <https://doi.org/10.3168/jds.2016-10865>.
- Kim YH, Nagata R, Ohkubo A, Ohtani N, Kushibiki S, Ichijo T, Sato S. 2018. Changes in ruminal and reticular pH and bacterial communities in Holstein cattle fed a high-grain diet. *BMC Vet Res* 14:310. <https://doi.org/10.1186/s12917-018-1637-3>.
- Steele MA, Croom J, Kahler M, AlZahal O, Hook SE, Plaizier K, McBride BW. 2011. Bovine rumen epithelium undergoes rapid structural adaptations during grain-induced subacute ruminal acidosis. *Am J Physiol Regul Integr Comp Physiol* 300:R1515–R1523. <https://doi.org/10.1152/ajpregu.00120.2010>.
- Liu JH, Xu TT, Liu YJ, Zhu WY, Mao SY. 2013. A high-grain diet causes massive disruption of ruminal epithelial tight junctions in goats. *Am J Physiol Regul Integr Comp Physiol* 305:R232–R241. <https://doi.org/10.1152/ajpregu.00068.2013>.
- Xu L, Wang Y, Liu J, Zhu W, Mao S. 2018. Morphological adaptation of sheep's rumen epithelium to high-grain diet entails alteration in the expression of genes involved in cell cycle regulation, cell proliferation and apoptosis. *J Anim Sci Biotechnol* 9:32. <https://doi.org/10.1186/s40104-018-0247-z>.
- Zebeli Q, Dunn SM, Ametaj BN. 2011. Perturbations of plasma metabolites correlated with the rise of rumen endotoxin in dairy cows fed diets rich in easily degradable carbohydrates. *J Dairy Sci* 94:2374–2382. <https://doi.org/10.3168/jds.2010-3860>.
- Ametaj BN, Emmanuel DG, Zebeli Q, Dunn SM. 2009. Feeding high proportions of barley grain in a total mixed ration perturbs diurnal patterns of plasma metabolites in lactating dairy cows. *J Dairy Sci* 92:1084–1091. <https://doi.org/10.3168/jds.2008-1465>.
- Li B, Zhang K, Li C, Wang X, Chen Y, Yang Y. 2019. Characterization and comparison of microbiota in the gastrointestinal tracts of the goat (*Capra hircus*) during preweaning development. *Front Microbiol* 10:2125. <https://doi.org/10.3389/fmicb.2019.02125>.
- Bekele AZ, Koike S, Kobayashi Y. 2011. Phylogenetic diversity and dietary association of rumen *Treponema* revealed using group-specific 16S rRNA gene-based analysis. *FEMS Microbiol Lett* 316:51–60. <https://doi.org/10.1111/j.1574-6968.2010.02191.x>.
- Ransom-Jones E, Jones DL, McCarthy AJ, McDonald JE. 2012. The Fibrobacteres: an important phylum of cellulose-degrading bacteria. *Microb Ecol* 63:267–281. <https://doi.org/10.1007/s00248-011-9998-1>.

27. Plaizier JC, Li S, Danscher AM, Derakshani H, Andersen PH, Khafipour E. 2017. Changes in microbiota in rumen digesta and feces due to a grain-based subacute ruminal acidosis (SARA) challenge. *Microb Ecol* 74: 485–495. <https://doi.org/10.1007/s00248-017-0940-z>.
28. Ogunade IM, McCoun M, Idowu MD, Peters SO. 2020. Comparative effects of two multispecies direct-fed microbial products on energy status, nutrient digestibility, and ruminal fermentation, bacterial community, and metabolome of beef steers. *J Anim Sci* 98:skaa201. <https://doi.org/10.1093/jas/skaa201>.
29. Wang X, Martin GB, Wen Q, Liu S, Li Y, Shi B, Guo X, Zhao Y, Guo Y, Yan S. 2020. Palm oil protects  $\alpha$ -linolenic acid from rumen biohydrogenation and muscle oxidation in cashmere goat kids. *J Anim Sci Biotechnol* 11: 100. <https://doi.org/10.1186/s40104-020-00502-w>.
30. Su XL, Tian Q, Zhang J, Yuan XZ, Shi XS, Guo RB, Qiu YL. 2014. *Acetobacteroides hydrogenigenes* gen. nov., sp. nov., an anaerobic hydrogen-producing bacterium in the family Rikenellaceae isolated from a reed swamp. *Int J Syst Evol Microbiol* 64:2986–2991. <https://doi.org/10.1099/ij.s.0.063917-0>.
31. Seshadri R, Leahy SC, Attwood GT, Teh KH, Lambie SC, Cookson AL, Eloe-Fadrosh EA, Pavlopoulos GA, Hadjithomas M, Varghese NJ, Paez-Espino D, Hungate1000 Project Orators, Perry R, Henderson G, Creevey CJ, Terrapon N, Lapebie P, Drula E, Lombard V, Rubin E, Kyrpides NC, Henrissat B, Woyke T, Ivanova NN, Kelly WJ. 2018. Cultivation and sequencing of rumen microbiome members from the Hungate1000 collection. *Nat Biotechnol* 36:359–367. <https://doi.org/10.1038/nbt.4110>.
32. Holman DB, Gzyl KE. 2019. A meta-analysis of the bovine gastrointestinal tract microbiota. *FEMS Microbiol Ecol* 95:fiz072. <https://doi.org/10.1093/femsec/fiz072>.
33. Youmans BP, Ajami NJ, Jiang ZD, Campbell F, Wadsworth WD, Petrosino JF, DuPont HL, Highlander SK. 2015. Characterization of the human gut microbiome during travelers' diarrhea. *Gut Microbes* 6:110–119. <https://doi.org/10.1080/19490976.2015.1019693>.
34. Jackson MA, Bonder MJ, Kuncheva Z, Zierer J, Fu J, Kurilshikov A, Wijmenga C, Zhernakova A, Bell JT, Spector TD, Steves CJ. 2018. Detection of stable community structures within gut microbiota co-occurrence networks from different human populations. *PeerJ* 6:e4303. <https://doi.org/10.7717/peerj.4303>.
35. Fernando SC, Purvis H, Najar F, Sukharnikov L, Krehbiel C, Nagaraja T, Roe B, DeSilva U. 2010. Rumen microbial population dynamics during adaptation to a high-grain diet. *Appl Environ Microbiol* 76:7482–7490. <https://doi.org/10.1128/AEM.00388-10>.
36. Weimer PJ. 2015. Redundancy, resilience, and host specificity of the ruminal microbiota: implications for engineering improved ruminal fermentations. *Front Microbiol* 6:296. <https://doi.org/10.3389/fmicb.2015.00296>.
37. Williams T, Morley J. 1973. Prostaglandins as potentiators of increased vascular permeability in inflammation. *Nature* 246:215–217. <https://doi.org/10.1038/246215a0>.
38. North JA, Miller AR, Wildenthal JA, Young SJ, Tabita FR. 2017. Microbial pathway for anaerobic 5'-methylthioadenosine metabolism coupled to ethylene formation. *Proc Natl Acad Sci U S A* 114:E10455–E10464. <https://doi.org/10.1073/pnas.1711625114>.
39. Packer L, Weber SU, Rimbach G. 2001. Molecular aspects of  $\alpha$ -tocotrienol antioxidant action and cell signalling. *J Nutr* 131:3695–3735. <https://doi.org/10.1093/jn/131.2.3695>.
40. Madeo F, Eisenberg T, Pietrocola F, Kroemer G. 2018. Spermidine in health and disease. *Science* 359:eaan2788. <https://doi.org/10.1126/science.aan2788>.
41. Sun FF, Cao YC, Cai CJ, Li SX, Yu C, Yao JH. 2016. Regulation of nutritional metabolism in transition dairy cows: energy homeostasis and health in response to post-ruminal choline and methionine. *PLoS One* 11: e0160659. <https://doi.org/10.1371/journal.pone.0160659>.
42. Zhang R, Zhu W, Jiang L, Mao S. 2017. Comparative metabolome analysis of ruminal changes in Holstein dairy cows fed low- or high-concentrate diets. *Metabolomics* 13:74. <https://doi.org/10.1007/s11306-017-1204-0>.
43. Saleem F, Ametaj BN, Bouatra S, Mandal R, Zebeli Q, Dunn SM, Wishart DS. 2012. A metabolomics approach to uncover the effects of grain diets on rumen health in dairy cows. *J Dairy Sci* 95:6606–6623. <https://doi.org/10.3168/jds.2012-5403>.
44. Kelly CJ, Zheng L, Campbell EL, Saeedi B, Scholz CC, Bayless AJ, Wilson KE, Glover LE, Kominsky DJ, Magnuson A, Weir TL, Ehrentauf SF, Pickel C, Kuhn KA, Lanis JM, Nguyen V, Taylor CT, Colgan SP. 2015. Crosstalk between microbiota-derived short-chain fatty acids and intestinal epithelial HIF augments tissue barrier function. *Cell Host Microbe* 17:662–671. <https://doi.org/10.1016/j.chom.2015.03.005>.
45. Mottawa W, Chiang C-K, Mühlbauer M, Starr AE, Butcher J, Abujamel T, Deeke SA, Brandel A, Zhou H, Shokralla S, Hajjibabaei M, Singleton R, Benchimol EI, Jobin C, Mack DR, Figeys D, Stintzi A. 2016. Altered intestinal microbiota-host mitochondria crosstalk in new onset Crohn's disease. *Nat Commun* 7:13419. <https://doi.org/10.1038/ncomms13419>.
46. Baserga R. 1968. Biochemistry of the cell cycle: a review. *Cell Prolif* 1: 167–191. <https://doi.org/10.1111/j.1365-2184.1968.tb00957.x>.
47. Goldberg AL, Stein R, Adams J. 1995. New insights into proteasome function: from archaeobacteria to drug development. *Chem Biol* 2:503–508. [https://doi.org/10.1016/1074-5521\(95\)90182-5](https://doi.org/10.1016/1074-5521(95)90182-5).
48. Bannink A, France J, Lopez S, Gerrits WJJ, Kebreab E, Tamminga S, Dijkstra J. 2008. Modelling the implications of feeding strategy on rumen fermentation and functioning of the rumen wall. *Anim Feed Sci Technol* 143: 3–26. <https://doi.org/10.1016/j.anifeeds.2007.05.002>.
49. Steele M, Dionissopoulos L, AlZahal O, Doelman J, McBride B. 2012. Rumen epithelial adaptation to ruminal acidosis in lactating cattle involves the coordinated expression of insulin-like growth factor-binding proteins and a cholesterolgenic enzyme. *J Dairy Sci* 95:318–327. <https://doi.org/10.3168/jds.2011-4465>.
50. Russell DW. 1992. Cholesterol biosynthesis and metabolism. *Cardiovasc Drugs Ther* 6:103–110. <https://doi.org/10.1007/BF00054556>.
51. Ma Y, Zhang Y, Zhang H, Wang H. 2021. Thiamine alleviates high-concentrate-diet-induced oxidative stress, apoptosis, and protects the rumen epithelial barrier function in goats. *Front Vet Sci* 8:663698. <https://doi.org/10.3389/fvets.2021.663698>.
52. Millen DD, Arrigoni MDB, Pacheco RDL (ed). 2016. *Rumenology*. Springer International Publishing, New York, NY.
53. Huntington GB, Zetina EJ, Whitt JM, Potts W. 1996. Effects of dietary concentrate level on nutrient absorption, liver metabolism, and urea kinetics of beef steers fed isonitrogenous and isoenergetic diets. *J Anim Sci* 74: 908–916. <https://doi.org/10.2527/1996.744908x>.
54. Baldwin RL, VI. 1998. Use of isolated ruminal epithelial cells in the study of rumen metabolism. *J Nutr* 128:293S–296S. <https://doi.org/10.1093/jn/128.2.293S>.
55. Oikonomou G, Valergakis G, Arsenos G, Roubies N, Banos G. 2008. Genetic profile of body energy and blood metabolic traits across lactation in primiparous Holstein cows. *J Dairy Sci* 91:2814–2822. <https://doi.org/10.3168/jds.2007-0965>.
56. National Research Council. 2011. *Guide for the care and use of laboratory animals*, 8th ed. National Academies Press, Washington, DC.
57. National Research Council. 2001. *Nutrient requirements of dairy cattle*, 7th revised ed. National Academies Press, Washington, DC.
58. Steele M, Schiestel C, AlZahal O, Dionissopoulos L, Laarman A, Matthews J, McBride B. 2015. The periparturient period is associated with structural and transcriptomic adaptations of rumen papillae in dairy cattle. *J Dairy Sci* 98:2583–2595. <https://doi.org/10.3168/jds.2014-8640>.
59. Xue M, Sun H, Wu X, Guan L, Liu J. 2019. Assessment of rumen bacteria in dairy cows with varied milk protein yield. *J Dairy Sci* 102:5031–5041. <https://doi.org/10.3168/jds.2018-15974>.
60. Magoč T, Salzberg SL. 2011. FLASH: fast length adjustment of short reads to improve genome assemblies. *Bioinformatics* 27:2957–2963. <https://doi.org/10.1093/bioinformatics/btr507>.
61. Rognes T, Flouri T, Nichols B, Quince C, Mahe F. 2016. VSEARCH: a versatile open source tool for metagenomics. *PeerJ* 4:e2584. <https://doi.org/10.7717/peerj.2584>.
62. Callahan BJ, McMurdie PJ, Rosen MJ, Han AW, Johnson AJA, Holmes SP. 2016. DADA2: high-resolution sample inference from Illumina amplicon data. *Nat Methods* 13:581–583. <https://doi.org/10.1038/nmeth.3869>.
63. Bolyen E, Rideout JR, Dillon MR, Bokulich NA, Abnet CC, Al-Ghalith GA, Alexander H, Alm EJ, Arumugam M, Asnicar F, Bai Y, Bisanz JE, Bittinger K, Brejnrod A, Brislawn CJ, Brown CT, Callahan BJ, Caraballo-Rodríguez AM, Chase J, Cope EK, Da Silva R, Diener C, Dorrestein PC, Douglas GM, Durall DM, Duvallet C, Edwards CF, Ernst M, Estaki M, Fouquier J, Gauglitz JM, Gibbons SM, Gibson DL, Gonzalez A, Gorlick K, Guo J, Hillmann B, Holmes S, Holste H, Huttenhower C, Huttley GA, Janssen S, Jarmusch AK, Jiang L, Kaehler BD, Kang KB, Keefe CR, Keim P, Kelley ST, Knights D, et al. 2019. Reproducible, interactive, scalable and extensible microbiome data science using QIIME 2. *Nat Biotechnol* 37:852–857. <https://doi.org/10.1038/s41587-019-0209-9>.
64. Bokulich NA, Kaehler BD, Rideout JR, Dillon M, Bolyen E, Knight R, Huttley GA, Gregory Caporaso J. 2018. Optimizing taxonomic classification of marker-gene amplicon sequences with QIIME 2's q2-feature-classifier plugin. *Microbiome* 6:90. <https://doi.org/10.1186/s40168-018-0470-z>.
65. Quast C, Pruesse E, Yilmaz P, Gerken J, Schweer T, Yarza P, Peplies J, Glöckner FO. 2013. The SILVA ribosomal RNA gene database project: improved data



- processing and Web-based tools. *Nucleic Acids Res* 41:D590–D596. <https://doi.org/10.1093/nar/gks1219>.
66. Weiss S, Xu ZZ, Peddada S, Amir A, Bittinger K, Gonzalez A, Lozupone C, Zaneveld JR, Vazquez-Baeza Y, Birmingham A, Hyde ER, Knight R. 2017. Normalization and microbial differential abundance strategies depend upon data characteristics. *Microbiome* 5:27. <https://doi.org/10.1186/s40168-017-0237-y>.
  67. Hartman K, van der Heijden MGA, Wittwer RA, Banerjee S, Walsler JC, Schlaeppi K. 2018. Cropping practices manipulate abundance patterns of root and soil microbiome members paving the way to smart farming. *Microbiome* 6:14. <https://doi.org/10.1186/s40168-017-0389-9>.
  68. Clauset A, Newman MEJ, Moore C. 2004. Finding community structure in very large networks. *Phys Rev E Stat Nonlin Soft Matter Phys* 70:066111. <https://doi.org/10.1103/PhysRevE.70.066111>.
  69. Bolger AM, Lohse M, Usadel B. 2014. Trimmomatic: a flexible trimmer for Illumina sequence data. *Bioinformatics* 30:2114–2120. <https://doi.org/10.1093/bioinformatics/btu170>.
  70. Kim D, Langmead B, Salzberg SL. 2015. HISAT: a fast spliced aligner with low memory requirements. *Nat Methods* 12:357–360. <https://doi.org/10.1038/nmeth.3317>.
  71. Anders S, Pyl PT, Huber W. 2015. HTSeq—a Python framework to work with high-throughput sequencing data. *Bioinformatics* 31:166–169. <https://doi.org/10.1093/bioinformatics/btu638>.
  72. Love MI, Huber W, Anders S. 2014. Moderated estimation of fold change and dispersion for RNA-seq data with DESeq2. *Genome Biol* 15:550. <https://doi.org/10.1186/s13059-014-0550-8>.
  73. Langfelder P, Horvath S. 2008. WGCNA: an R package for weighted correlation network analysis. *BMC Bioinformatics* 9:559. <https://doi.org/10.1186/1471-2105-9-559>.
  74. Yu G, Wang L-G, Han Y, He Q-Y. 2012. clusterProfiler: an R package for comparing biological themes among gene clusters. *OMICS* 16:284–287. <https://doi.org/10.1089/omi.2011.0118>.
  75. Sokal RR, Rohlf FJ. 1995. *Biometry: the principles and practice of statistics in biological research*. WH Freeman & Co, New York, NY.